Low-Frequency Domain Motions in the Carboxy Terminal Fragment of L7/L12 Ribosomal Protein Studied with Molecular Dynamics Techniques: Are These Movements Model Independent?

Yves-Henri Sanejouand*,† and Orlando Tapia‡

Laboratoire d'Enzymologie Physico-chimique et Moléculaire, Bât. 430, Université Paris Sud, 91405 Orsay, France, and Department of Physical Chemistry, University of Uppsala, Box 532, S-75121 Uppsala, Sweden

Received: July 28, 1994; In Final Form: January 13, 1995⊗

A large-amplitude and low-frequency (5-cm^{-1}) domain−domain motion is found to occur in two molecular dynamics simulations of the carboxy terminal fragment of the L7/L12 ribosomal protein of *E. coli*. These simulations were carried out at constant energy with the CHARMM program package (ref 1), with two different electrostatic protocols: one in which a "smoothed" 9-Å cutoff is used and another one in which all atom−atom interactions are taken into account. Our results are in agreement with those obtained previously from the analysis of simulations performed with another electrostatic protocol, another kind of trajectory initialization, another kind of statistical ensemble, another program package, etc. (refs 2−4). This ensemble of results suggests that the low-frequency domain−domain motion we observe is unlikely to be an artifact due to the particularities of the protocols used to perform all of these simulations. It is much more likely to be a dynamical characteristic of the particular fold of the carboxy terminal fragment of the L7/L12 ribosomal protein.

Introduction

The carboxy terminal fragment (CTF) of the L7/L12 ribosomal protein is essential for efficient polypeptide synthesis in bacteria[5]—it appears to be the key constituent for elongation-factor-dependent GTPase activity.[6] In previous molecular dynamics (MD) studies of the CTF dimer (which had been shown to be the ultimate functional unit), a collective motion between the oligomers was characterized.[3] Moreover, it was shown that this dynamical property of the CTF dimer reflects one of the most striking features of the dynamical behavior of the monomer, *i.e.*, a low-frequency motion (around 5 cm^{-1}) that is performed by two of its (sub)domains; this motion appears as a fluctuation of relatively large amplitude of the αα domain with respect to the β-sheet domain.[2,4] Interestingly, the residues of the regions involved in this concerted motion are highly conserved in different species.[4]

By now, it is quite apparent that molecular simulation techniques can provide important information on the dynamical properties of proteins at the atomic level.[7] For instance, they were used to demonstrate that high-frequency atomic fluctuations make possible the diffusion of dioxygen from the surface of the rather compact myoglobin molecule toward the iron site.[8,9] More generally, they give useful insights on the relationship between the dynamical fluctuation pattern of proteins and their biological properties.[10] One question to answer now concerns the reliability MD techniques have to predict functionally significant motions.

In Åqvist *et al.* MD simulations of CTF, the GROMOS program package was used. While invariance of dynamical behavior as a function of environmental parameters, *e.g.*, solvent effects and dimer interactions, was addressed, no attempt to examine force-field invariance was done. This is one of the issues to be examined in this paper. This is all the more important since MD techniques rely on the assumption that the Born−Oppenheimer potential energy surface of macromolecules can be accurately approximated by analytical potential energy functions. Insofar as parameters are concerned, such representations are far from being unique—there are several classical force fields used in various program packages. Furthermore, the type of simulation differs in most applications: microcanonical ensemble conditions are used by some authors; others rely on open thermal systems with temperature controls such as in the GROMOS package, while other groups may prefer the use of grand canonical ensemble conditions. Here, the CHARMM program package is employed.[1] The initial conditions, parameters, and cutoffs in the electrostatic part of the potential function are all different from those used before by other groups; microcanonical ensemble conditions are used. The hypothesis underlying this report is simply stated as follows: if collective motions of domains are characteristic of the folded form of CTF, they should be independent of models used to carry out the MD simulations.

Model and Methods

From the MD practical point of view, the CTF monomer is a very attractive model. Since it is a small protein (64 residues), otherwise costly studies are allowed, like normal mode analysis,[11] long trajectories in water,[12] and denaturation studies.[13] Also, CTF is an extremely well-folded protein with a high degree of regular secondary structures (approximately 76% of the protein, arranged in the following sequence: β-A−α-A−α-B−β-B−α-C−β-C); the existence of well-defined secondary structures is very convenient for analysis purposes, since a given configuration can be described in a simple way, in terms of a few rigid body parameters.

(i) Simulations. The potential energy function has the same form in the CHARMM and GROMOS programs but the CTF topology files are somewhat different: for GROMOS, there are 336 dihedrals and 263 improper dihedrals in CTF, while for CHARMM there are 360 and 239 of them, respectively. The

* Present address: Laboratoire de Physique Quantique, U.R.A. 505 of C.N.R.S., I.R.S.A.M.C., Université Paul-Sabatier, 118 route de Narbonne, 31062 Toulouse Cedex, France.
† Université Paris Sud.
‡ University of Uppsala.
⊗ Abstract published in *Advance ACS Abstracts,* March 15, 1995.

0022-3654/95/2099-5698$09.00/0

TABLE 1: Differences between CHARMM and GROMOS Backbone Partial Charges

atom	CHARMM	GROMOS
N	−0.35	−0.28
H	+0.25	+0.28
Cα	+0.10	0.00
C	+0.55	+0.38
O	−0.55	−0.38

TABLE 2: Neutralization of CHARMM Charged Groups

residue	atomic name	CHARMM charges	modified charges
N-ter	HT	+0.35	+0.25
	N	−0.30	−0.75
	CA	+0.25	0.00
Lys	CE	+0.25	0.00
	NZ	−0.30	−0.75
	HZ	+0.35	+0.25
Arg	CD	+0.10	0.00
	NE	−0.40	−0.25
	HE	+0.30	+0.25
	CZ	+0.50	0.00
	NH	−0.45	−0.50
	HH	+0.35	+0.25
Asp	CB	−0.16	0.00
	CG	+0.36	+0.72
	OD	−0.60	−0.36
Glu	CG	−0.16	0.00
	CD	+0.36	+0.72
	OE	−0.60	−0.36
C-ter	C	+0.14	+0.72
	OT	−0.57	−0.36

two programs differ also, and mainly, in their set of parameters[1,2,14]—a comparison of CHARMM and GROMOS backbone partial charges is given in Table 1. However, in order to describe the same collisionless solvent model used in previous simulations with GROMOS, the partial charges of NH_3^+ and COO^- groups have been screened in such a way that they add up to zero;[2] thus, 129 of the 596 CHARMM atomic charges for CTF have been modified (see Table 2).

Åqvist *et al.* simulations were constant-temperature ones; a simple, sharp, 8-Å cutoff for the electrostatic interactions was used. In the present study, constant energy calculations are performed, which are much more sensitive to discontinuities in the potential energy function. Thus, in a first simulation, a SWITCH cutoff for the van der Waals forces (between 7 and 9 Å) and a SHIFT cutoff (9 Å) for the electrostatic interactions are used.[1] Since it has been shown that the low-frequency regime of the theoretically calculated density of states depends upon particular electrostatic cutoff procedures,[15] a second simulation has been performed, during which all atom-pair interactions are calculated. In this case, each potential energy value requires the calculation of 176 796 interactions instead of around 45 000 interactions for the other trajectory.

Before each simulation, the X-ray structure[16] has been thoroughly minimized with Powell's algorithm, the average gradient being used as convergence criterion instead of the energy. In both cases, the process was stopped after about 4000 steps at a root-mean-square value of 0.0001 kcal/(mol·Å).

The initial velocities were assigned by using a method based on canonical directions[17] derived from normal mode analysis,[18] as explained hereafter.

In the normal mode analysis, one considers the expansion of the potential energy function, $V(\boldsymbol{u})$, around a stationary point in terms of the fluctuation variables $\Delta\boldsymbol{u} = \boldsymbol{u} - \boldsymbol{u}_0$, where $\boldsymbol{u}_0$ stands for the coordinates of the stationary structure. Up to second order in $\Delta\boldsymbol{u}$,

$$V(\boldsymbol{u}) = {}^1/_2\Delta\boldsymbol{u}^t\cdot\mathbf{F}\Delta\boldsymbol{u}$$

where $\mathbf{F}$ is the mass-weighted second-derivative matrix of the potential energy. Introducing the kinetic and potential energies in the Lagrangian ($L = K - V$), the Euler−Lagrange equation of motion is

$$\Delta\ddot{\boldsymbol{u}} = -\mathbf{F}\cdot\Delta\boldsymbol{u}$$

where a double dot indicates a second-order derivative with respect to time. These equations are solved by using the ansatz

$$\Delta\boldsymbol{u} = \mathbf{A}\cdot\boldsymbol{q}$$

where the components of the normal mode vector $\boldsymbol{q}$ are given by $q_i = C_i \cos(\omega_i t + \phi_i)$, where ω_i is the pulsation, C_i the amplitude, and ϕ_i the phase of the time-dependent component of the ith mode. The two latter parameters depend upon initial conditions. The canonical directions matrix $\mathbf{A}$ is the orthogonal transformation diagonalizing $\mathbf{F}$, *i.e.*,

$$\mathbf{A}^t\cdot\mathbf{F}\cdot\mathbf{A} = \mathbf{\Lambda}$$

where $\mathbf{\Lambda}$ is the diagonal matrix whose elements are equal to the square of ω_i and where $\mathbf{A}^t$ is the transposed form of $\mathbf{A}$.

Sloane and Hase proposed to set the initial atomic velocities $\boldsymbol{v}$ in MD trajectories according to[17]

$$\boldsymbol{v} = \mathbf{M}^{1/2}\mathbf{A}\dot{\boldsymbol{q}}$$

where $\mathbf{M}$ is the diagonal atomic masses matrix.

Each element of the $\dot{\boldsymbol{q}}$ vector, the normal mode velocities vector, may be chosen so as to have an initial kinetic energy of k_bT on each normal mode (k_b is the Boltzmann constant and T is the "target" temperature for the simulation). Note that with this procedure a simulation can start without a smooth heating up. Moreover, there is no need of randomly generate initial velocities, as is often the case in standard simulations; the deterministic character of simulations may thus be reinforced, in the sense that initial conditions are more likely to be completely specified; this may help further comparative studies.

In order to use the Sloane and Hase method, prior to each of our simulations, the force constant matrix $\mathbf{F}$ was numerically calculated in the mass-weighted Cartesian frame with a central difference algorithm. In order to get canonical directions free from spurious overall rotation or translation, $\mathbf{F}$ was first projected according to the Williams method.[11,19]

In both of our simulations, the target temperature was set to 270 K, close and below the thermal bath temperature used by Åqvist *et al.* (277 K). Verlet's algorithm was used to integrate the equations of motion; in Åqvist *et al.*'s work, a leap-frog algorithm was employed. As has been shown elsewhere, both algorithms should produce equivalent trajectories.[2]

A 1-fs integration time step was used except during the first picosecond where a 0.5-fs time step was used. The nonbonded list was updated every 5 fs. In order to constrain bond distances all along our 65-ps trajectories, SHAKE[20] was applied with a tolerance of 10^{-3} Å. Note that the average temperature of our simulations was not controlled by periodic rescaling. This allows us to get direct information about the evolution of the molecule on the potential energy surface toward deeper minima. It also increases the deterministic character of our simulations, in the sense specified above.

(ii) Analysis. Atom dynamics in well-folded proteins, such as the carboxy terminal fragment of the L7/L12 ribosomal protein (Figure 1), appears to an observer as more or less random fluctuations around equilibrium positions. Concerted dynamical

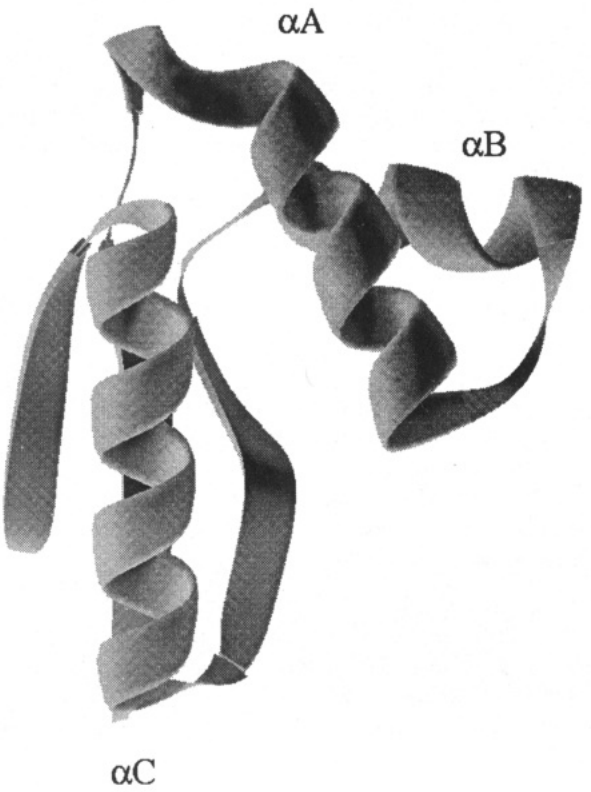

Figure 1. Ribbon representation of the C terminal fragment (residues 53−120) of the L7/L12 ribosomal protein. The sequence of secondary structure elements is β-A−α-A−α-B−β-B−α-C−β-C. The loop connecting the helices α-A and α-B forms a β-strand that extends the β-sheet of the second monomer.

behavior involving secondary structures or particular subdomains must be extracted from the time series of atom coordinates by calculating, for instance, correlation functions from time series of angles between pairs of α-helical axes, while frequencies for such types of concerted atomic motions can be obtained with fast Fourier transform (FFT) techniques.

In order to obtain significant results, helical stabilities have to be checked all along the trajectories. Following Colonna−Cesari's algorithm,[21] local helical axes are calculated by using four consecutive Cα, from i to $i + 3$, and by fitting them to an ideal helical section. Gliding along an α-helix, the consecutive axis should be parallel. Helical breaking points can be detected with this technique as the angle between consecutive axes attains a value larger than 25°. This defines a kink. Such a choice of limiting kink angle value corresponds to the largest fluctuations found in the core of the CTF's helices. In some helices, the kink angle value was overrun at its ends and the computed helices had to be shortened (see below).

Results and Discussion

(i) MD Trajectory with Cutoff. The X-ray crystallographic structure (XRS) has been minimized as described above. The rms difference between the minimized structure and the XRS one is 1.25 Å, when all atoms are taken into account, while it is 0.71 Å when only Cα atoms are. During minimization, the angles between helical axes change by about 2−4°.

The initial temperature is twice the target temperature, *i.e.*, 540 K, and it attains a value of 270.2 ± 9.0 K during the second picosecond, the kinetic energy introduced at the beginning being transformed into potential energy according to the equipartition energy principle (this statement is certainly true for the high-frequency motions which contribute the most to the kinetic energy, but the low-frequency motions might not yet have attained equilibration, *i.e.*, their relative phases may not yet have reached a random distribution). All along the simulation, the temperature slowly and regularly increases; between 20 and 25 ps, the average temperature is 291.0 ± 8.3 K; in the range 25−65 ps, the temperature is fairly constant, reaching the average temperature of 293.9 ± 8.7 K between 60 and 65 ps.

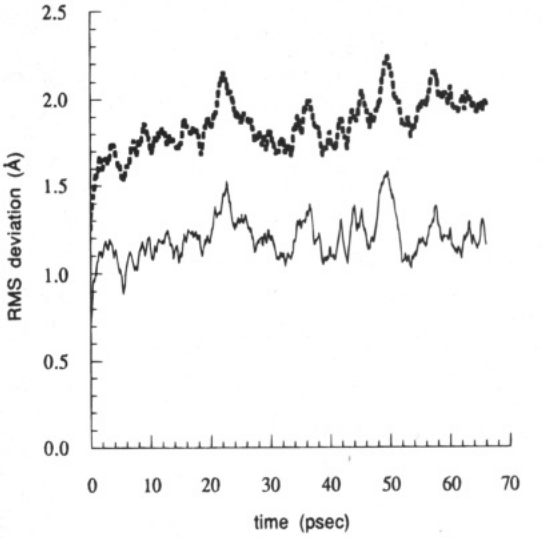

Figure 2. Cα atoms (continuous line) and all-atom (dashed line) root-mean-square deviation from the crystal structure, during the 9-Å cutoff simulation, as a function of time.

On the one hand, our results show that overall equilibration is attained at about 20 ps, a result in agreement with the Åqvist *et al.* simulation;[2] analysis will be done from this point onward. On the other hand, they show that, at the end of this trajectory, the system has reached a zone of the global potential energy function having a minimum with lower energy than the starting structure. This produces a temperature drift between 1 and 20 ps. The 2-deg increment in the temperature between 20 and 65 ps is explained by a total energy drift from −1743.4 up to −1738.3 kcal/mol during the simulation. This effect is probably due to a cutoff effect, as will be documented in the trajectory run without cutoff.

The time evolution of the Cα and all-atom rms deviations of the CTF from the XRS are depicted in Figure 2. After a few picoseconds, the value of the Cα rms deviation fluctuates around 1.2 Å, while the all-atom one fluctuates around 1.9 Å. These values are slightly smaller than those obtained by Åqvist *et al.* (1.3 and 2.1 Å, respectively).

(a) Comparisons of MD and X-ray Results. The Cα rms differences between the XRS and the average MD structure are depicted in Figure 3. As one may expect in this type of simulation, the loops show significant deviations. Differences larger than 1.2 Å are found in the loops between β-A and α-A (residues 62−65), α-B and β-B (residues 88 to 90), and β-B and α-C (residues 97, 99, and 100). Otherwise, the differences are below 0.8 Å for most of the Cα atoms of the secondary structure elements.

The β-A−α-A loop displacement from the XRS is notoriously larger than 1.2 Å. A similar result was found in Åqvist *et al.*'s simulation. The reason for this effect is probably found in the absence of the sulfate counterion and "fixed" water molecules, which are present in the crystal and missing in both simulations, as has been shown by simulations including water and counterions.[22]

The loop between α-B and β-B deviates in a manner similar to the one found in Åqvist *et al.*'s simulation. Differences among both simulations are also detected, but they do not alter the overall agreement found at this level.

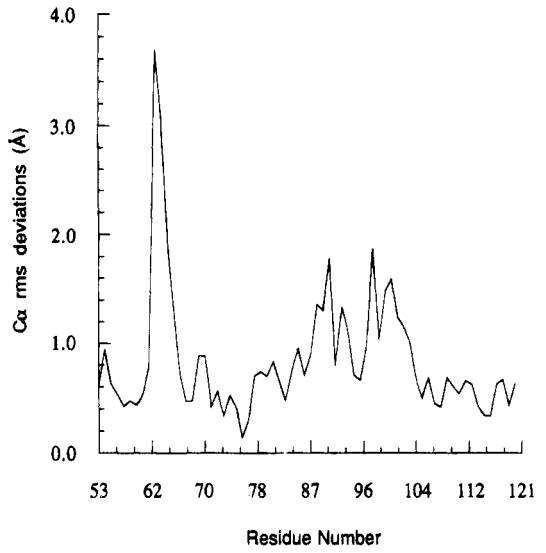

Figure 3. Cα root-mean-square deviations from the crystal structure during the 9-Å cutoff simulation, as a function of residue number. The residues are numbered as in the L7/L12 protein, starting from residue 53.

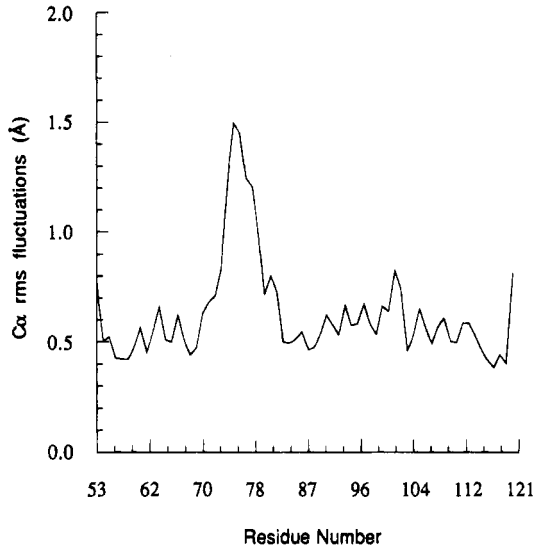

Figure 4. Cα root-mean-square fluctuations around the 20−65-ps averaged structure, during the 9-Å cutoff simulation, as a function of residue number.

In Figure 4, Cα rms fluctuations are reported. There, only loop regions have fluctuations larger than average (0.63 Å). In particular, the loop between α-A and α-B presents the largest atomic fluctuations—some of its Cα positions fluctuate by 1.2−1.5 Å. As expected, these values are larger than those corresponding to the experimental *B* factors (around 0.7 Å)—in the XRS, this loop is a part of the second oligomer β-sheet.

In other loops, rms fluctuations were larger in Åqvist *et al.*'s simulation (between 0.8 and 1.0 Å). This may be due to the fact that the trajectory studied in the present work is shorter than the one reported by those authors (65 against 150 ps); it is possible that the loops did not have enough time to sample the same portion of the conformational space.

(b) Helical Motions. The definition used in X-ray crystallography to quality as an α-helix was not found to be satisfactory when analyzing the present MD trajectory. In fact, here, the ends of the crystallographically defined helices fluctuate in such a way that the kink angle attains values of 63°, 27°, and 38° for α-A (residues 64−77), α-B (residues 79−88), and α-C (residues 99−113), respectively.

TABLE 3: Average Helical Parameters[a]

helix	pitch, Å	pitch ange, deg	radius, Å	kink, deg
A	1.61 ± 0.27	99.5 ± 9.0	2.25 ± 0.26	22
B	1.52 ± 0.20	98.8 ± 5.9	2.29 ± 0.20	21
C	1.50 ± 0.23	99.3 ± 8.7	2.32 ± 0.24	21

[a] Ideal helix parameters are pitch = 1.50 Å, pitch angle = 100.0°, radius = 2.30 Å.

By excluding four N-terminal residues and three C-terminal residues, α-A is defined hereafter by residues 66−74, with a maximal kink angle of 23°, α-B by residues 80−88, with a maximal kink angle of 21°, and α-C by residues 100−113, with a 21° maximum kink angle—in Table 3, the average pitch, radius, and pitch angle and the average errors on their determination are given for the three helices. The entries of this table show that α-B and α-C, as they are defined above, are quite regular helices all along the trajectory. Even though α-A is less regular, its helical parameters deviating most from those of an ideal α-helix, the three helical axes are well-defined objects whose relative angles can be calculated as a function of time with great accuracy.

Åqvist *et al.*'s results have shown that α-B is involved in low-frequency motions and that its quasi-periodic fluctuations are more clearly displayed when α-C is used to sense the relative motion—α-C being tightly bound to the β-sheet, it has not the possibility to librate as the helices making the αα corner[23] do. Thus, in Figure 5, only the times series for the angles between α-B and α-C, the corresponding correlation function, and relative power spectra are depicted.

The ensemble of results shows that α-B is involved in low-frequency motions, being similar to what can be expected from Åqvist *et al.*'s results for a shorter simulation, *i.e.*, the spectrum not being as sharply centered around 5 cm^{-1}. Moreover, they provide additional evidence that low-frequency fluctuations may be invariant with respect to simulation conditions.

(ii) MD Trajectory without Cutoff. For the sake of comparison with the previous trajectory, the same initial structure, *i.e.*, the XRS, was energy minimized. However, the minimum attained differs from the one obtained above. The rms difference from the XRS is now 1.2 Å, when all atoms are taken into account, and 0.8 Å when only Cα are. Thus, already at this level the change in cutoff produces a difference. The time evolution of the Cα and all-atom rms deviations of the CTF from the XRS are depicted in Figure 6. These deviations slowly attain, in about 30 ps, and then fluctuate around, an average value of respectively 1.4 and 2.2 Å; these values are of similar size to those obtained by Åqvist *et al.*

In the time range between 30 and 65 ps, the temperature fluctuates around 290 K. In the time range between 20 and 25 ps, the temperature already has an average value of 288 K. Note that for the present trajectory there is no temperature drift after the 30-ps point. There, the total energy is virtually perfectly conserved, the difference between the last and first steps amounting to 0.4 kcal/mol.

(a) Comparison of MD and X-ray Results. The Cα rms differences between the XRS and the average MD structure are depicted in Figure 7. Differences larger than 1.6 Å are found in the loops between β-A and α-A and α-A and α-B. The β-A−α-A loop displacement from the XRS is much larger than 1.2 Å for the three considered monomer trajectories; this reinforces the reason given before, namely, that this large displacement originates in the absence of counterions and fixed water molecules which are present in the crystal and missing in all three simulations.

At variance with the previous trajectory, there is a large shift of the loop connecting α-A to α-B; this shift was also present

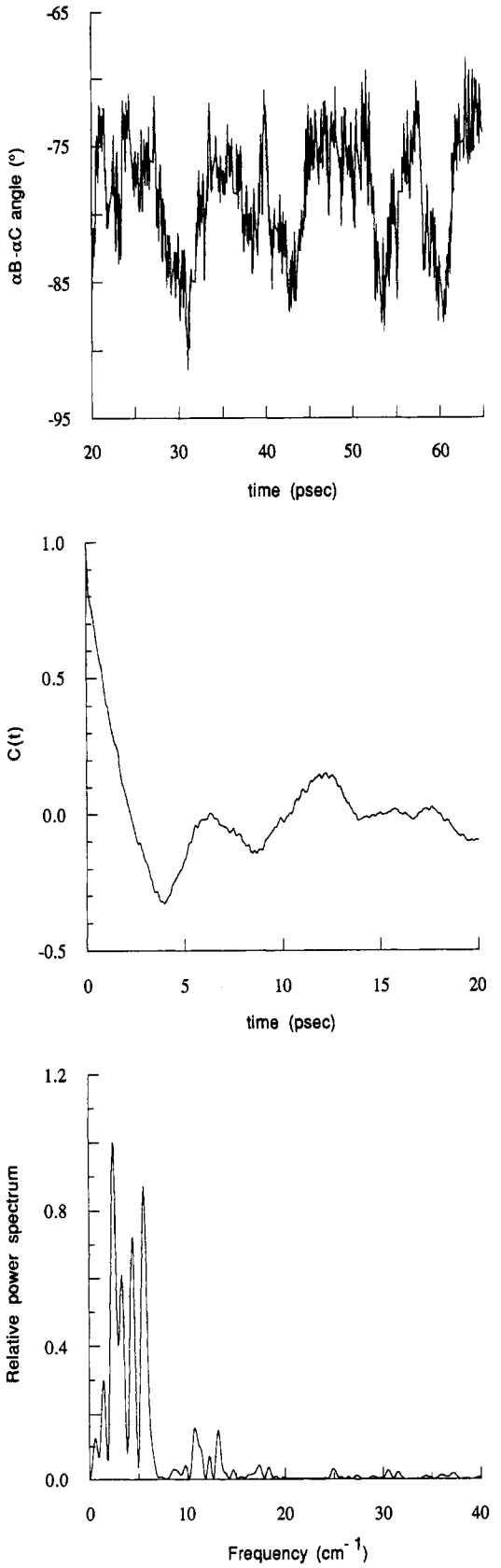

Figure 5. Relative displacement of α-B and α-C helical axis during the 9-Å cutoff simulation. (a) Time series of the angle between the helical axis; (b) corresponding time correlation function; (c) corresponding relative power spectrum.

in Åqvist *et al.*'s study. The point of highest deviation is found at the end of helix α-A. Actually, the axis of α-A has changed with respect to the XRS by about 10°, thereby eliciting a change in the relative position of the α−α corner. The deviation is

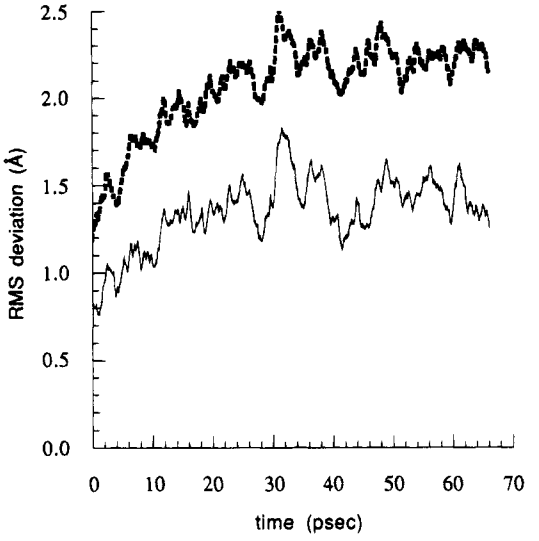

Figure 6. Cα atoms (continuous line) and all-atom (dashed line) root-mean-square deviation from the crystal structure, during the all-interaction simulation, as a function of time.

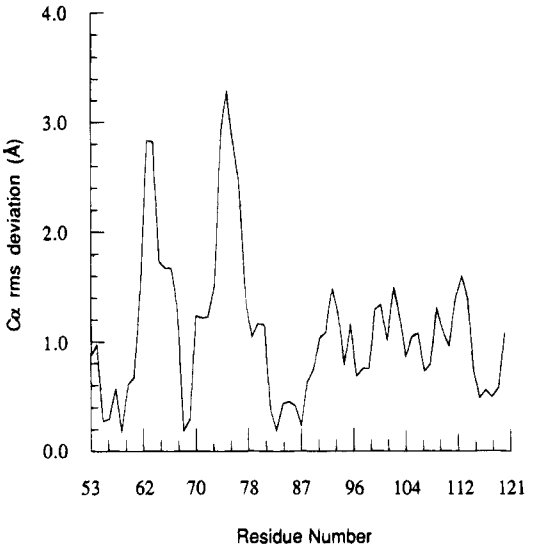

Figure 7. Cα root-mean-square deviations from the crystal structure during the all-interaction simulation, as a function of residue number.

damped at the end of the loop. One possible explanation is that such a conformational change is rare enough to have occurred only once in two over the three considered simulations; in the remaining simulation, the previous one, it may have occurred more often since this loop was found to fluctuate a lot.

Note that structurally, even if there are local differences, the overall folding pattern of CTF is conserved in all three averaged MD structures.

In Figure 8, Cα fluctuations are reported. All loop regions have fluctuations slightly larger than 0.6 Å. The loop between α-A and α-B, which had the largest atomic fluctuations in the previous trajectory, now has much smaller values; this reinforces the above hypothesis. On the other hand, the values of atomic fluctuations have ranges fairly similar to those shown by experimental *B* factors. The dynamical properties found in the present trajectory can thus be considered as quite satisfactory.

In fact, averaged structural information obtained from all three considered simulations are in similar, and good, agreement with experimental data. Moreover, a similar agreement was found with a 200-ps water simulation[12] computed with a different program package, ENCAD.[24] Thus, though our simulations are much shorter and without any explicit water molecules, they

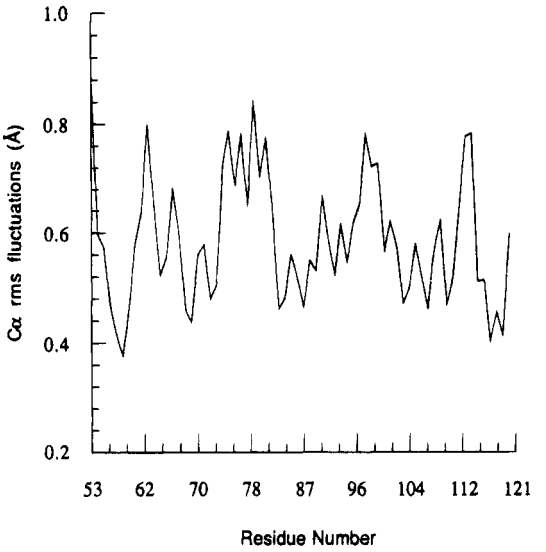

Figure 8. Cα root-mean-square fluctuations around the 20–65-ps averaged structure, during the all-interaction simulation, as a function of residue number.

lead to results as good as other approaches and representative of CTF-averaged dynamical properties. Furthermore, these results, obtained by three different program packages, are found not to be sensitive to the choice of a particular force field.

(b) Helical Motions. The limits used to define helices in the preceding trajectory have been retained here. The maximum kink angles are now smaller than those found above. They range between 16° (α-C) and 20° (α-B). The average pitch of the three helices is now 1.57, 1.54, and 1.51 Å for α-A, α-B, and α-C, respectively. These entries are slightly better than the previous ones; noteworthy, the α-A helix looks more stable in the present simulation.

The time series for the angle made by helices α-B and α-C is depicted in Figure 9, together with its correlation function and its relative power spectrum. The time series is far from being white noise, and the fluctuations of the α-B–α-C angle clearly elicit dominating low-frequency motions—the correlation function shows by its slow decrease the presence of this type of motion. The power spectrum confirms this picture. However, it is more complex than the ones from previous simulations. This may be due to the fact that here equilibration took place on a longer time span. From the energetic point of view, it lasts around 30 ps, at variance with the previous 20-ps estimates. From the helical motion point of view (see Figure 9), the equilibration period may not have been over until 40–45 ps.

Final Remarks

A low-frequency domain motion in CTF has been shown to be conserved under a number of different simulation conditions. This intradomain fluctuation has been found now in a microcanonical ensemble framework; since Åqvist *et al.*'s simulations were made at constant temperature, one could have suspected that the thermal bath used there to maintain the temperature was the cause for the CTF dynamical behavior. Our results show that it is not the case.

Such a validation study of time-dependent MD results is still rare. To the best of our knowledge, the only extensive study of this type was done by comparing normal modes computed for crambin with various program packages.[25] Though of great interest, such a study addressed low-temperature dynamical properties only, *i.e.*, the temperature domain of validity of the normal modes approximation.

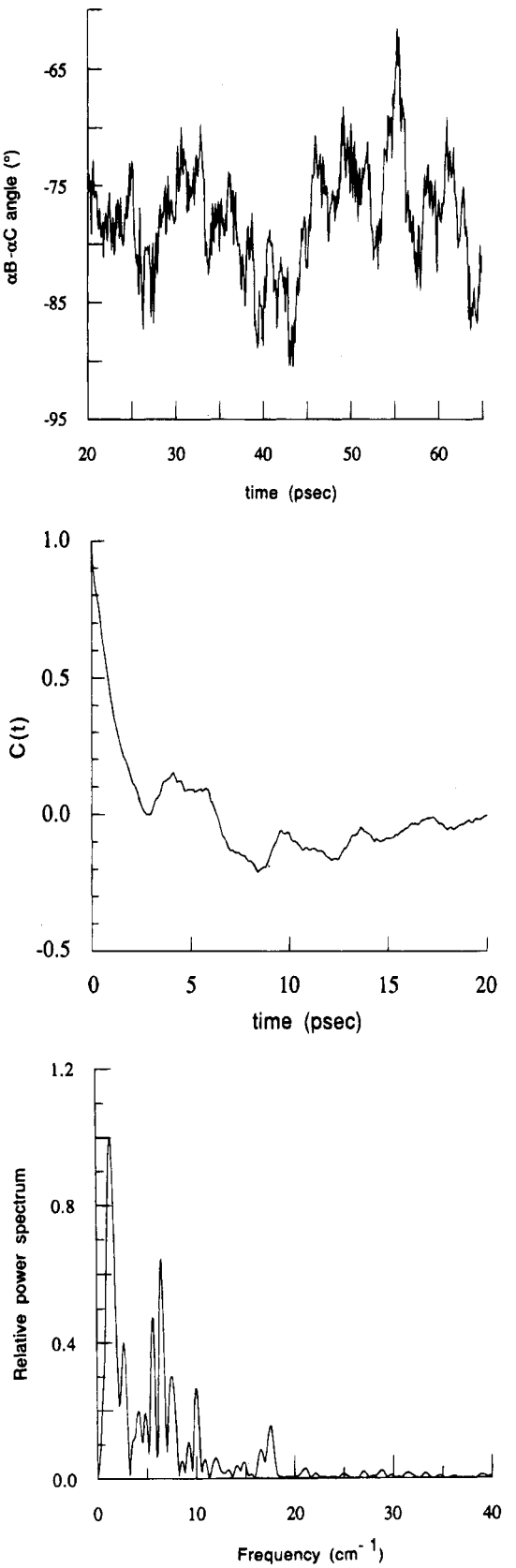

Figure 9. Relative displacement of α-B and α-C helical axis during the all-interaction simulation. (a) Time series of the angle between the helical axis; (b) corresponding time correlation function; (c) corresponding relative power spectrum.

Sensitivity to various electrostatic procedures has been checked more often in the literature. However, conclusions seem to vary from model to model.[15,25,26] Here, though equilibration was slowed by the long-distance interactions

taken into account in our second simulation, CTF also exhibited low-frequency domain motions. However, a longer simulation would be necessary to confirm that detailed characteristics, like amplitude and frequency, are conserved.

The present work contributes to show that a low-frequency domain motion is a dynamical consequence of CTF tertiary structure. Since more and more data are now becoming available on the protein biosynthesis machinery, noteworthy, on elongation factors structures,[27-29] such a result could well, in the near future, be important to build up a detailed understanding of how this complex system actually works.

References and Notes

(1) Brooks, B. R.; Bruccoleri, R. E.; Olafson, B. D.; States, D. J.; Swaminathan, S.; Karplus, M. *J. Comp. Chem.* **1983**, *4*, 187.
(2) Åqvist, J.; van Gunsteren, W. F.; Leijonmarck, M.; Tapia, O. *J. Mol. Biol.* **1985**, *83*, 461.
(3) Åqvist, J.; Leijonmarck, M.; Tapia, O. *Eur. Biophys. J.* **1989**, *16*, 327.
(4) Tapia, O.; Nilsson, O.; Campillo, M.; Åqvist, J.; Horjales, E. In *Structure & Methods, DNA Protein Complexes*; Sarma, R. H., Sarma, M. H., Eds.; Adenine: New York, 1990; Vol. 2, p 147.
(5) Möller, W. In *Ribosomes*; Nomura, M., Tissieres, A., Lengyel, P., Eds.; Cold Spring Harbor Laboratory: Cold Spring Harbor, NY, 1974; p 711.
(6) Möller, W.; Groene, A.; Terhorst, C.; Amons, P. *Eur. J. Biochem.* **1972**, *25*, 5.
(7) Brooks, C. L.; Pettit, B. M.; Karplus, M. *Adv. Chem. Phys.* **1988**, *71*, 1.
(8) Perutz, M. F.; Matthews, F. S. *J. Mol. Biol.* **1966**, *21*, 199.
(9) Case, D. A.; Karplus, M. *J. Mol. Biol.* **1979**, *132*, 343.
(10) Gurd, F. R. N.; Rothgeb, T. M. *Adv. Protein Chem.* **1979**, *33*, 73.
(11) Sanejouand, Y. H. Ph.D. Thesis, Orsay University, Orsay, France, 1990.
(12) Daggett, V.; Levitt, M. *Chem. Phys.* **1991**, *158*, 501.
(13) Daggett, V. In *Techniques in protein chemistry*; Angeletti, R. H., Eds.; Academic: New York, to be published.
(14) van Gunsteren, W. F.; Berendsen, H. J. C. *Groningen Molecular Simulation (GROMOS) Library Manual*; BIOMOS B.V.: Nijenborgh 16, Groningen, The Netherlands, 1987.
(15) Smith, J.; Kuczera, K.; Tidor, B.; Doster, W.; Cusack, S.; Karplus, M. *Physica B* **1989**, *156–157*, 437.
(16) Leijonmarck, M.; Liljas, A. *J. Mol. Biol.* **1987**, *195*, 555.
(17) Sloane, C. S.; Hase, W. L. *J. Chem. Phys.* **1977**, *66*, 1523.
(18) Goldstein, H. *Classical Mechanics*; Addison Wesley: Reading, MA, 1950.
(19) Williams, I. H. *J. Mol. Struct.* **1983**, *94*, 275.
(20) Ryckaert, J.-P.; Ciccotti, G.; Berendsen, H. J. C. *J. Comp. Phys.* **1977**, *23*, 327.
(21) Colonna-Césari, F. Personal communication, 1990.
(22) Åqvist, J.; Tapia, O. *Biopolymers* **1990**, *30*, 205.
(23) Efimov, A. *FEBS Lett.* **1984**, *166*, 33.
(24) Levitt, M. Ph.D. Thesis, Stanford University, Los Angeles, 1990.
(25) Teeter, M. M.; Case, D. A. *J. Phys. Chem.* **1990**, *94*, 8091.
(26) Loncharich, R. J.; Brooks, B. *Proteins* **1989**, *6*, 32.
(27) Kjeldgaard, M.; Nyborg, J. *J. Mol. Biol.* **1992**, *223*, 721.
(28) Kjeldgaard, M.; Nissen, P.; Thirup, S.; Nyborg, J. *Structure* **1993**, *1*, 35.
(29) Berchtold, H.; Reshetnikova, L.; Reiser, C. O. A.; Shirmer, N. K.; Sprinzl, M.; Hilgenfeld, R. *Nature* **1993**, *365*, 126.

JP941967Q